AGU PUBLICATIONS

Geophysical Research Letters

RESEARCH LETTER
10.1002/2017GL076451

**Key Points:**
- We model global seasonal horizontal and vertical surface displacements induced by loading derived from GRACE in a viscoelastic framework
- We show that viscosities derived to explain early postseismic deformation may yield a detectable effect on horizontal seasonal displacements
- Asthenospheric viscosity lower bound from seasonal deformation suggesting some postseismic studies cannot hold for the global average

**Supporting Information:**
- Supporting Information S1

**Correspondence to:**
K. Chanard,
kristel.chanard@ign.fr

**Citation:**
Chanard, K., Fleitout, L., Calais, E., Barbot, S., & Avouac, J.-P. (2018). Constraints on transient viscoelastic rheology of the asthenosphere from seasonal deformation. *Geophysical Research Letters*, *45*. https://doi.org/10.1002/2017GL076451

Received 18 NOV 2017
Accepted 7 FEB 2018
Accepted article online 12 FEB 2018

©2018. American Geophysical Union. All Rights Reserved.

# Constraints on Transient Viscoelastic Rheology of the Asthenosphere From Seasonal Deformation

**Kristel Chanard[1,2,3], Luce Fleitout[2], Eric Calais[2], Sylvain Barbot[4], and Jean-Philippe Avouac[3]**

[1]LASTIG LAREG, IGN, ENSG, Université Paris Diderot, Sorbonne Paris Cité, Paris, France, [2]Laboratoire de Géologie, Ecole Normale Supérieure/CNRS UMR 8538, PSL Research University, Paris, France, [3]Division of Earth and Planetary Sciences, California Institute of Technology, Pasadena, CA, USA, [4]Department of Earth Sciences, University of Southern California, Los Angeles, CA, USA

**Abstract** We discuss the constraints on short-term asthenospheric viscosity provided by seasonal deformation of the Earth. We use data from 195 globally distributed continuous Global Navigation Satellite System stations. Surface loading is derived from the Gravity Recovery and Climate Experiment and used as an input to predict geodetic displacements. We compute Green's functions for surface displacements for a purely elastic spherical reference Earth model and for viscoelastic Earth models. We show that a range of transient viscoelastic rheologies derived to explain the early phase of postseismic deformation may induce a detectable effect on the phase and amplitude of horizontal displacements induced by seasonal loading at long wavelengths (1,300–4,000 km). By comparing predicted and observed seasonal horizontal motion, we conclude that transient asthenospheric viscosity cannot be lower than $5 \times 10^{17}$ Pa.s, suggesting that low values of transient asthenospheric viscosities reported in some postseismic studies cannot hold for the seasonal deformation global average.

## 1. Introduction

Campaign and continuous Global Navigation Satellite System (GNSS) monitoring around fault zones are often used to characterize patterns of the earthquake cycle, delimiting and measuring coseismic, postseismic, and interseismic deformation. However, although transient strains have been systematically observed in the years or decades following large earthquakes (Burgmann & Dresen, 2008; Thatcher & Pollitz, 2008), constitutive laws governing the spatial and time-dependent postseismic deformation remain an ongoing debate. Effective asthenospheric viscosities of a few $1.10^{18}$ Pa.s, typically $3.10^{18}$ Pa.s, are necessary to explain the observed postseismic deformation after a few years following a large event (Trubienko et al., 2014). In addition, velocities recorded by continuous GNSS stations during the first months following major earthquakes are faster than predicted using such viscosities (Figure S1 in the supporting information) (Pollitz et al., 2006; Trubienko et al., 2014). Several mechanisms have been proposed to explain those observations: (1) rapidly decaying slip on the ruptured fault or in its vicinity, commonly referred to as afterslip (Barbot et al., 2009; Fialko, 2004; Freed, 2007; Klein et al., 2016; Marone et al., 1991; Perfettini & Avouac, 2004; Savage et al., 1994), a mechanism often favored for explaining near-field observations (Ingleby & Wright, 2017), and (2) viscoelastic relaxation of coseismic stresses in the lower crust and upper mantle, with multiple relaxation times and/or stress-dependent viscosities (Chandrasekhar et al., 2009; DeVries & Meade, 2013; Freed & Bürgmann, 2004; Pollitz, 2003; Pollitz & Thatcher, 2010; Pollitz et al., 2006; Ryder et al., 2011; Trubienko et al., 2014). Identifying the respective contributions of these various mechanisms is challenging but is key to a better understanding of the seismic cycle and to the potential link between aftershocks and postseismic deformation.

A type of model of postseismic deformation, where only viscoelastic relaxation is considered, employs a linear viscoelastic Burgers rheology (Pollitz, 2003), a rheology supported by rock physics experiments (Chopra, 1997; Hanson & Spetzler, 1994; Raj, 1975; Post, 1977; Sigmundsson, 1991; Sun et al., 2014) and by mechanical models based on homogenization (Ivins, 1996). The model includes transient and steady state viscosities, to reproduce observations of both the early and later stage of postseismic stages. For example, Pollitz (2003) used a biviscous Burgers rheology in the lower crust and shallow subcrustal mantle to model rapid early deformation

and the longer-term relaxation, following the M7.1 Hector Mine, California, earthquake, with an estimated transient viscosity of $1.6\times10^{17}$ Pa.s, corresponding to a relaxation time of about a month. Other studies found comparable transient viscosity values for mega-earthquakes inducing deformation over more than 1,000 km, able to sample the mechanical properties of the upper mantle: $5\times10^{17}$ Pa.s (Pollitz et al., 2006), $4\times10^{17}$ Pa.s (Gunawan et al., 2014; Mikhailov et al., 2013) following the 2004 Sumatra-Andaman earthquake, $2\times10^{17}$ Pa.s after the 2006–2007 Kuril earthquakes (Kogan et al., 2013), or $2.5\times10^{17}$ Pa.s after the 2010 Tohoku earthquake (Sun et al., 2014).

The linear viscoelastic rheology of the asthenosphere, defined here in relation to its mechanical properties at shallow depth, derived from these postseismic studies must be compatible with other loading sources at comparable spatiotemporal scales. In particular, they should be consistent with the seasonal deformation of the Earth, mainly due to continental water storage and nontidal ocean and atmospheric masses (Blewitt et al., 2001; Van Dam et al., 2001). Indeed, far-field stress perturbations ($\geq$500 km from the epicenter) within the asthenosphere used to infer asthenospheric viscosities from postseismic deformation (velocities of 5 mm/yr due to strain relaxation in a 200 km thick asthenosphere with a viscosity of $3.10^{18}$ Pa.s) are comparable to the stress perturbations due to seasonal loading (of order of 1 kPa) so that the physical mechanisms of deformation should be the same for the two processes. Note that nonlinear rheologies are not considered here because stresses involved in both processes are negligible compared to background tectonic stresses.

In many geophysical processes, a form of transient creep is present in relation with attenuation, from seismic to annual or even multiannual time scales. In most cases, these processes involve a low-amplitude plastic deformation, smaller than the elastic deformation induced by the associated stresses (Anderson et al., 1965; Bos et al., 2015; Smith & Dahlen, 1981). However, the asthenospheric creep we aim to detect using the seasonal deformation mode involves plastic deformations larger than the elastic one.

Other studies have used surface load variations to probe the Earth's viscoelastic rheology at a range of spatiotemporal scales: filling or draining of large lakes (Bills & May, 1987; Bills et al., 2007; Doin et al., 2015) or postglacial isostatic rebound (Lambeck et al., 1998; Larsen et al., 2005; Sigmundsson, 1991). Here we explore this idea at the annual time scale by comparing seasonal deformation from 195 globally distributed continuous Global Navigation Satellite System (cGNSS) stations to the predictions of viscoelastic models with various rheological properties of the asthenosphere, loaded by mass variations derived from satellite gravity measurements provided by the Gravity Recovery and Climate Experiment (GRACE) (Bettinelli et al., 2008; Chanard, 2015; Chanard et al., 2014; Fu & Freymueller, 2012; Fu et al., 2012, 2013; Nahmani et al., 2012).

## 2. Seasonal Variations of Surface Loading and Seasonal Ground Displacement

### 2.1. Surface Mass Variations Derived From GRACE

We use global mass redistribution at the Earth surface estimated from gravity measurements by the satellite mission GRACE (Tapley et al., 2005), from 2002 to 2012. We use 10 day Level-2 solutions produced by the Centre National d'Etudes Spatiales (CNES)/Groupe de Recherches de Géodésie Spatiale (GRGS) (http://grgs.obsmip.fr/), to which we add back the atmospheric and nontidal oceanic loading contribution (Carrère & Lyard, 2003). Solutions are expressed in terms of Stokes coefficients representing the residual gravitational effects, then converted to water mass coefficients (millimeter of equivalent water height (EWH)) by isotropic filtering (Ramillien et al., 2005). We interpolate 10 day 1-by-1 degree grids of water mass from the water mass coefficients and remove a time average from each 10 day solution so that the solutions are expressed with respect to the mean solution over the time span of analysis. Time series of EWH are detrended and empirically corrected for detectable coseismic and postseismic gravity changes due to mega-earthquakes (Chanard, 2015; Chen et al., 2007; Han et al., 2006, 2008; Ogawa & Heki, 2007). As the degree-1 loads are not observed by GRACE, we account for their contribution as described by Chanard (2015). We invert the residuals between GNSS time series and GRACE derived displacements, for each model of Earth, induced by loads of spherical harmonic degree $\geqslant 2$ for a degree-1 deformation field together with a net translation (and a net rotation), which aims to accommodate misalignments of the GNSS solution to the theoretical reference frame. Note that the harmonics of very low degree-2 and degree-3 of the gravity field solutions cannot be estimated accurately by GRACE and are stabilized in the CNES/GRGS solutions using LAser GEOdynamics Satellite orbits (Lemoine et al., 2007). Figure 1 shows the averaged annual peak-to-peak amplitude of the EWH in millimeter for the 2002–2012 time period. The corresponding EWH time series are used as an input loading function for deformation models.

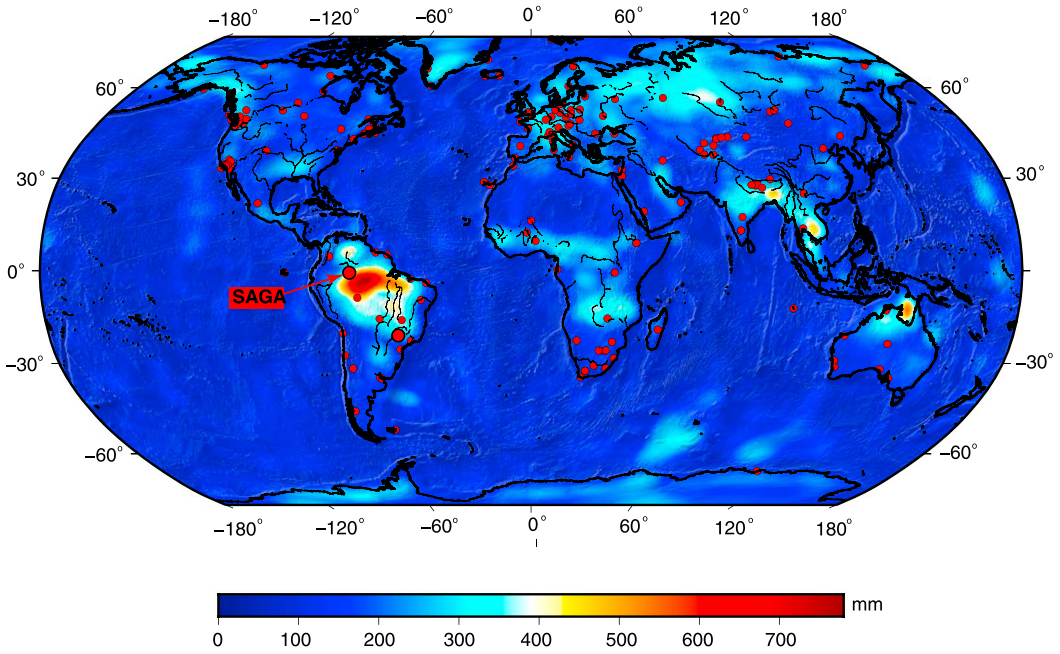


**Figure 1.** Peak-to-peak surface load variations, expressed in equivalent water height (in millimeters), derived from Gravity Recovery and Climate Experiment for the 2002–2012 period and corrected from detectable earthquakes coseismic contributions. Red dots show location of the continuous Global Navigation Satellite System stations used in this study.

### 2.2. GNSS Data Set

We use daily position time series from continuous GNSS stations as provided by the Nevada Geodetic Laboratory (http://geodesy.unr.edu). Note that this is an arbitrary choice of strategy processing. Differences in processing techniques, particularly in the choice of mapping functions, can reach up to a millimeter for the vertical component (Steigenberger et al., 2009) but do not affect significantly horizontal displacements, and our final results will rely on horizontal components exclusively.

We favor stations of the International GNSS Service network to obtain reliable time series at a globally distributed network of sites with observation time span longer than 4 years. This leads to 452 sites from which we further select a subset of 173 sites where time series show a clear seasonal signal with no significant data gap. We include an additional 28 sites that are not part of the International GNSS Service but are located in areas where strong seasonal displacements are expected and have long (≥4 years) and continuous time series. The location of the 195 stations used in this study is shown in Figure 1. To extract nontectonic signals $D_s$ of a GNSS time series $D$, we model and remove from the raw time series: (i) their initial position $D(t_0)$; (ii) steady velocity $V(t-t_0)$; (iii) potential earthquake coseismic and postseimic (with characteristic time $\tau$, determined from postseismic studies of each modeled earthquake) contributions; and (iv) known material change jumps:

$$D_s(t) = D(t) - D(t_0) + V(t-t_0) + \sum_i a_i \mathcal{H}(t-t_i) + \sum_i b_i \mathcal{H}(t-t_i) \ln\left(1 + \frac{t-t_i}{\tau}\right) + \sum_j c_j \mathcal{H}(t-t_j), \quad (1)$$

where the ($a_i$, $b_i$, and $c_j$) account, respectively, for the coseismic, postseismic, and material change corrections. We remove outliers beyond 3 times the interquartile range of the median on any of the three components. Note that we estimate annual, semiannual, and draconitic signals up to the sixth harmonic from the 195 GNSS station position time series and remove the estimated draconitic signals from the time series. Finally, we compute a 10 day weighted average that coincides with the GRACE temporal sampling. Figure 2 shows the daily position time series at station SAGA (Brazil) together with the cleaned, 10 day averaged, time series. This station, located in the Amazon basin where large annual fluctuations of EWH are observed (Figure 2), shows peak-to-peak annual displacements of 30 mm on the vertical and 10 mm on the horizontal. A selection of additional stations is displayed in Figures S2 and S3.

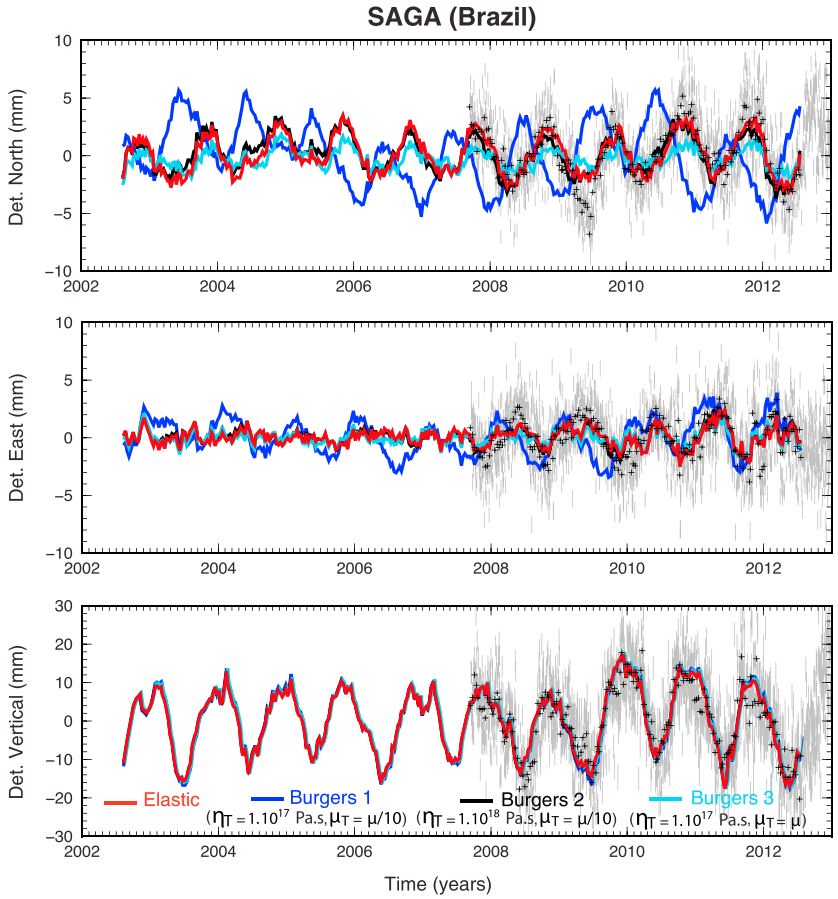


**Figure 2.** Daily detrended geodetic positions, error bars for $1\sigma$ uncertainties (gray), and 10 day moving average (black crosses) determined at continuous Global Navigation Satellite System station SAGA (location in Figure 1). Predicted displacements induced by Gravity Recovery and Climate Experiment-derived seasonal surface loading derived are shown for a purely elastic model (red) and Burgers 1 (blue), where $\eta_T = 1.10^{17}$ Pa.s, $\eta = 1.10^{19}$ Pa.s, and $\mu_T = \mu/10$ between 70 and 270 km depth; Burgers 2 (black), where $\eta_T = 1.10^{18}$ Pa.s, $\eta = 1.10^{19}$ Pa.s, and $\mu_T = \mu/10$ between 70 and 270 km depth; and Burgers 3 (light blue), where $\eta_T = 1.10^{17}$ Pa.s, $\eta = 1.10^{19}$ Pa.s, and $\mu_T = \mu$ between 70 and 270 km depth. In all models, degree-1 and reference frame issues have been addressed as proposed by Chanard (2015).

## 3. Global Modeling of Seasonal Ground Deformation Induced by Surface Load Variations

### 3.1. Description of the Model

We compute surface displacements induced by variations of surface loading using a numerical model based on a spherical harmonics and temporal frequencies decomposition of the GRACE-derived loads that uses the Love number theory. Surface loads, $\mathcal{L}(t, \theta, \phi)$, varying with time ($t$), longitude ($\theta$), and latitude ($\phi$), are decomposed into loads, $\hat{\mathcal{L}}(\omega, l, m)$, varying with temporal frequency ($\omega$) and spherical harmonics of degree and order ($l$, $m$) (Caron et al., 2017; Craig et al., 2016). We compute surface displacements induced by a unit load for each spherical harmonic of the decomposition and each frequency of the load (Figure 1) by a system of equations for the deformation of a self-gravitational spherical body, similar to classical normal modes theory used in seismology. Love numbers are frequency-dependent complex Love numbers when considering viscoelastic rheologies and frequency-independent real numbers in the elastic case. We then combine displacements for each frequency, when necessary, and spherical harmonic to obtain surface displacements induced by the global surface loading at time $t$, longitude $\theta$, and latitude $\phi$.

### 3.2. The Purely Elastic Case

We use the preliminary reference Earth model (PREM) structure (Dziewonski & Anderson, 1981), where the oceanic crust is replaced by a continental crust (Bassin, 2000), to compute load Love numbers and Green's functions for horizontal and vertical displacements caused by an annual, unit, harmonic loading

function (Figure S4). Note that the choice of the Earth's elastic structure is arbitrary as surface displacements induced by the long wavelengths loads reliably detected by the GRACE mission (≥700 km) will not be sensitive to elastic variations within the crust where models differ significantly (Figure S4). We then convolve the Green's functions with the spatially and temporally varying surface load derived from GRACE from 2002 to 2012, compute model surface displacements at the selected set of continuous GNSS stations and compare model results to geodetic observations. This approach has been previously used to compute the Earth's response to seasonal loading derived from various hydrological models (Blewitt et al., 2001; Van Dam et al., 2001) or from GRACE observations (Bettinelli et al., 2008; Chanard, 2015; Chanard et al., 2014; Davis et al., 2004; Fu & Freymueller, 2012; Fu et al., 2012). The fit to observations for the vertical component is usually good (with mean weighted root-mean-square reduction of ∼50% for set of globally distributed GNSS sites) but the horizontal component is often poorly predicted (with a mean weighted root-mean-square reduction of a few % only). Chanard (2015) shows that predictions of horizontal components can be significantly improved by estimating the degree-1 deformation field from a comparison between the GRACE-derived model, with no a priori degree-1 loads, and observations rather than using published degree-1 coefficients derived from other techniques. Figure 2 shows, for example, that the model position time series at site SAGA matches well the observations for all three components. In particular, the horizontal component is well reproduced, both in amplitude and in phase. See supporting information Figure S3 for similar plots at other sites.

## 4. Potentially Detectable Asthenosphere Transient Viscoelastic Rheology From Seasonal Loading

We now test the effect of modifying the elastic model by including a viscoelastic asthenosphere with parameters in the range of typical values derived from postseismic studies. In this section, surface displacements induced by annual harmonic loads for elastic and for various viscoelastic Earth models are compared. We consider models with an elastic lithosphere of thickness $H_e$ with a linear elastic behavior on top of a viscoelastic asthenosphere of thickness $H$ and an underlying mantle (Figure 3a). Our calculations show that even with relatively low values of mantle viscosity ($10^{19}-10^{20}$ Pa.s), the model predictions are similar to an elastic response at an annual loading period. Thus, our models use a mantle below the asthenosphere of constant Maxwell viscosity of $10^{20}$ Pa.s and PREM elastic parameters.

We use a Burgers rheology in the asthenosphere described by a bulk modulus $\kappa$, a transient viscosity and shear modulus $\eta_T$ and $\mu_T$, and a steady state viscosity and elastic shear modulus $\eta$ and $\mu$ (Figure 3a). We fixed the steady state elastic parameters to the PREM values and the associated steady state viscosity to $10^{19}$ Pa.s as lower values would not be compatible with inferences of long-term asthenospheric viscosities from convective heat transfer (Dumoulin et al., 1999). The relaxation time associated with the long-term viscosity is therefore much longer than the annual loading frequency and thus is not a dominant model parameter. Note that the commonly used Maxwell rheology for longer term deformation is an end-member of the Burgers rheology, where $\eta_T \rightarrow \infty$, or $\mu_T \rightarrow \infty$, or $\mu_T << \mu_{\text{elastic}}$. In the last case, the Burgers rheology is equivalent to a Maxwell rheology with an effective viscosity such that $1/\eta_{\text{eff}} = 1/\eta + 1/\eta_T$.

Examples of model results are illustrated in Figure 3. We chose a value of the transient viscosity of $1\times10^{17}$ Pa.s, at the lower end of the range of tested values, to enhance the effect of the asthenospheric viscosity on seasonal amplitude and phase shift. Our model shows that for spherical harmonic degrees from 10 to 30 (or loading wavelengths 1,300–4,000 km), a transient viscosity of $\eta_T = 10^{17}$ Pa.s, with $\mu_T = \mu$ in a 70–270 km depth Burgers asthenosphere would decrease the amplitude of horizontal seasonal surface displacement and induce a phase lag of about 30 days, while the vertical displacements would remain close to those predicted by a purely elastic model for the low harmonics degree dominating the GRACE data (Figure 3b). We also observe that a transient shear modulus of $\mu_T = \mu/10$, with $\eta_T = 10^{17}$ Pa.s in a 70–270 km depth Burgers asthenosphere, comparable to a Maxwell rheology with an effective viscosity $\sim10^{17}$ Pa.s, would, on the contrary, amplify seasonal horizontal signals at the 10–30 spherical harmonic degrees and create a time lag up to 3 months between elastic and viscoelastic seasonal horizontal displacements, while vertical predictions would remain similar (Figure 3c).

Finally, a reduced asthenospheric layer thickness $H$ would reduce differences between elastic and viscoelastic models (Figure 3d) at all spherical harmonic orders. Note that the thickness of $H_e$ does not influence the response to long wavelength loads captured by GRACE but rather acts as a filter for small wavelength

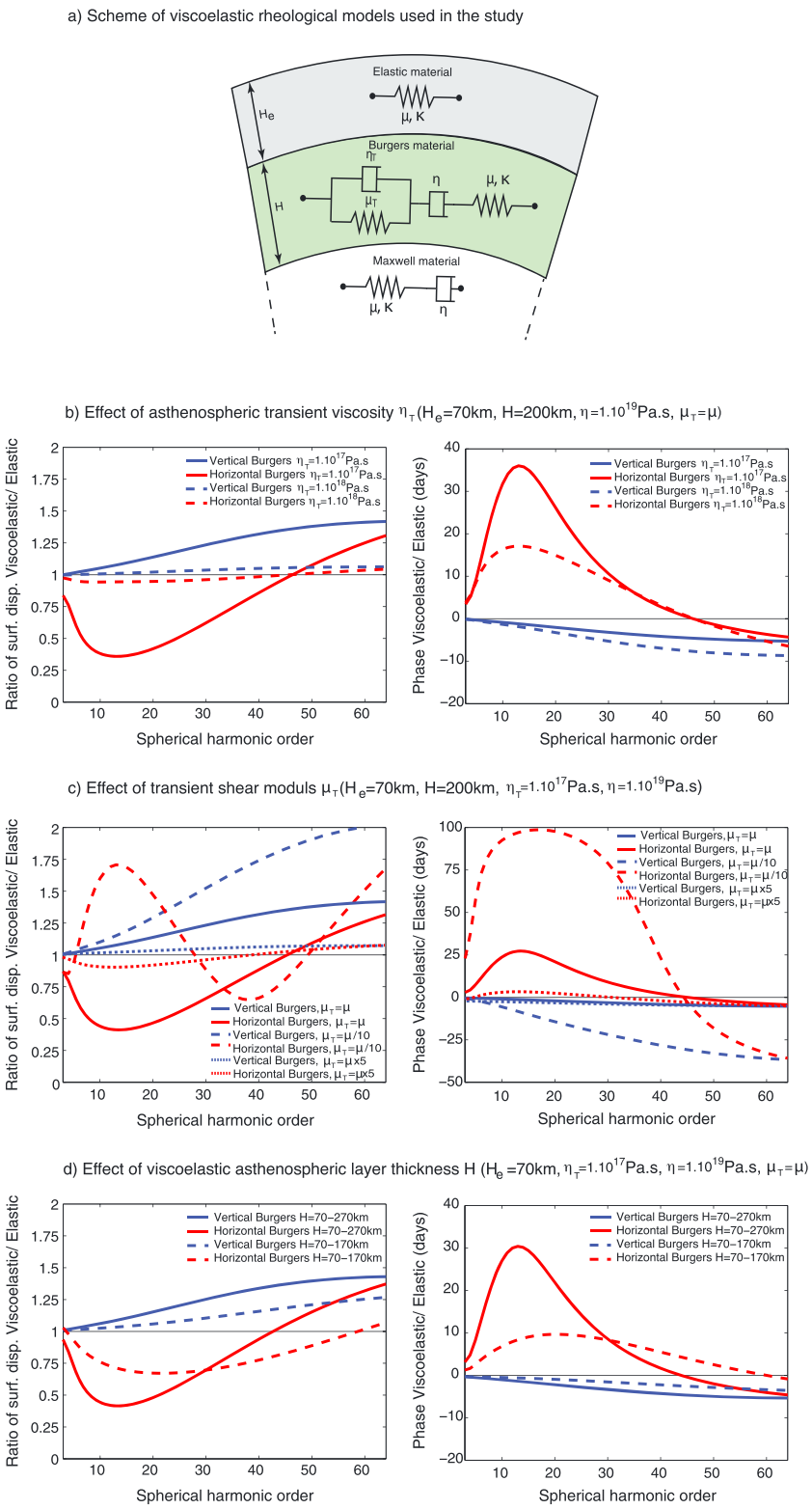


**Figure 3.** (a) Scheme of viscoelastic model used in our study, including an elastic lithosphere of thickness $H_e$, an asthenosphere of thickness $H$ with a Burgers rheology characterized by a transient viscosity and shear modulus $\eta_T$ and $\mu_T$, and a steady state viscosity and shear modulus $\eta$ and $\mu$. The underlying mantle has a Maxwell rheology. (b–d) Ratio of surface displacements and phase lag between viscoelastic models with a Burgers asthenospheric rheology and a purely elastic model for vertical (blue) and horizontal (red) components, induced by a 1 year periodic unit harmonic loading function obtained respectively using a viscoelastic model. (b) shows the effect of $\eta_T$, (c) $\mu_T$, and (d) $H$.

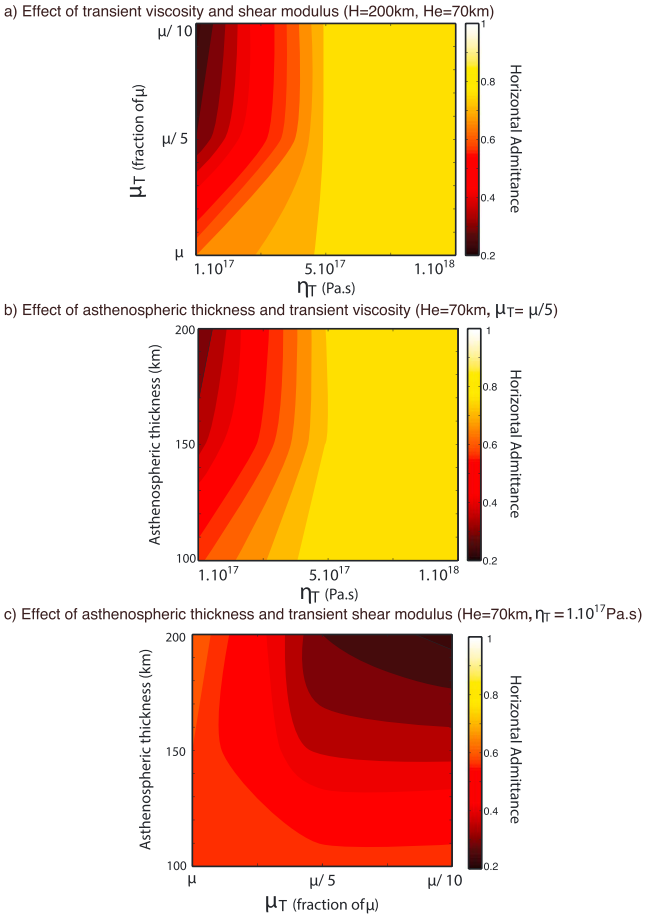


**Figure 4.** Maps of mean horizontal admittance (see equation (2)) between observations at 195 continuous Global Navigation Satellite System stations globally distributed and Gravity Recovery and Climate Experiment-derived viscoelastic seasonal models as a function of model parameters (see Figure 3). Transient viscosities in the asthenosphere lower than $5.10^{17}$ Pa.s, a transient shear modulus lower that $\mu/5$, and a thickness greater than 100 km appear rather unlikely to model accurately global horizontal seasonal displacements observed at continuous Global Navigation Satellite System stations and induced by seasonal loading derived from Gravity Recovery and Climate Experiment.

harmonic loads (Figure S6). Therefore, we discard the elastic thickness $H_e$ as a first-order parameter in the following analysis.

Thus, low transient viscosity derived from postseismic studies based on a Burgers rheology may induce a detectable signature in the annual deformation of the Earth driven by surface load variations at long wavelengths, from 1,000 to 4,000 km, seen in the GRACE time series and the seasonal deformation mode may help constraining postseismic rheologies.

## 5. Constraints on Transient Viscoelastic Parameters From Seasonal Global Deformation

We compute the horizontal and vertical surface displacements at the set of 195 cGNSS stations described in section 2.2 for a range of models for Earth models including a viscoelastic asthenosphere with a Burgers rheology and submitted to variations of surface loading derived from GRACE over the period 2002–2012. The comparison of the observed and predicted signal at site SAGA shown in Figure 2 indicates that the Burgers 2 model ($\eta_T = 10^{18}$ Pa.s) predicts reasonably well both the horizontal and vertical components. This comes from the fact that independent from the transient shear modulus values, the combination of an asthenospheric $10^{18}$ Pa.s transient viscosity and a $10^{19}$ Pa.s steady state viscosity (or here the equivalent Maxwell rheology with an effective viscosity of $9\times10^{17}$ Pa.s) behaves similarly to a purely elastic rheology under annual loading. When the model includes a lower transient viscosity of a few $10^{17}$ Pa.s in the asthenosphere, its response varies significantly depending on the transient shear modulus value. When $\mu_T << \mu$ (Burgers 1), the asthenosphere rheology becomes equivalent to a Maxwell body, resulting in horizontal displacements overestimated in amplitude and 3 months in advance compared to observations, while the predicted vertical displacements remain close to the elastic model. When $\mu_T = \mu$ (Burgers 3), the model is in phase with observations but horizontal amplitudes are underestimated. These conclusions hold for all stations located in areas of a strong hydrological loading signal (Figures S2 and S3). Therefore, the horizontal component of seasonal deformation is the one that contains the most useful information on the transient rheology of the asthenosphere. In addition, as the vertical seasonal component is likely to contain significant other geophysical signals (poroelastic, thermoelastic effects), we will focus our study exclusively on the horizontal components.

To quantify globally how well the model predicts the horizontal seasonal displacements, we evaluate the scalar admittance at each station $i$ and for each component $j$ (east, north) between $N_i$ observations and predictions as follows:

$$A_{i,j} = \frac{\sum_{k=1}^{N_i} d_{i,j,k}.m_{i,j,k}}{\sum_{k=1}^{N_i} (m_{i,j,k})^2}, \quad (2)$$

**Table 1**
*Summary of Earth Transient Viscoelastic Rheologies With Values of Transient Viscosities $\eta_T$ and Transient Shear Modulus $\mu_T$ in the Asthenosphere (70–200 km Depth) as Presented in Figure 2*

| Model | Color | Transient viscosity $\eta_T$ (Pa.s) | Transient shear modulus $\mu_T$ |
|---|---|---|---|
| Burgers 1 | blue | $1 \times 10^{17}$ | $\mu/10$ |
| Burgers 2 | black | $1 \times 10^{18}$ | $\mu/10$ |
| Burgers 3 | cyan | $1 \times 10^{17}$ | $\mu$ |

*Note.* All models have a steady state viscosity $\eta$ of $1 \times 10^{19}$ Pa.s and elastic shear modulus $\mu$.

**Table 2**
*Mean, Median, and Standard Deviation (Std) of East and North Admittance as Defined by Equation (2) for Various Rheological Models*

| | East admittance | | | North admittance | | |
|---|---|---|---|---|---|---|
| Model | Mean | Median | Std | Mean | Median | Std |
| Elastic | 1.09 | 0.890 | 0.142 | 1.12 | 1.01 | 0.157 |
| Burgers 1 | 0.434 | 0.321 | 0.203 | 0.446 | 0.301 | 0.199 |
| Burgers 2 | 0.941 | 0.881 | 0.155 | 0.959 | 0.891 | 0.163 |
| Burgers 3 | 0.583 | 0.514 | 0.161 | 0.621 | 0.603 | 0.148 |

*Note.* Models parameters are summarized in Table 1.

where $A_{ij}$ corresponds to the least squares regression coefficient of the observed versus modeled displacements, $d_{i,j,k}$ and $m_{i,j,k}$ the observed and modeled displacement at station $i$, for component $j$, and at time $k$, respectively. It corresponds to the factor by which the model has to be multiplied in order to achieve the best least squares fit to the data. The model is exact when the admittance equals 1, and under and over predicts the observations when the admittance is smaller or larger than 1, respectively. The purely elastic model leads to an horizontal admittance of 1.1, indicative of good fit to the observations, although amplitudes are underestimated by 10%.

The global horizontal admittance as a function of model parameters, shown in Figure 4, highlights that when the transient shear modulus is smaller than the elastic one, a transient viscosity of at least $5 \times 10^{17}$ Pa.s, for a reasonably thick asthenosphere (100 to 200 km) is required to globally fit the load-induced seasonal displacements observed in cGNSS time series. This result is confirmed by statistics on global admittance; results are given in Table 2, with associated maps in Figure S6.

## 6. Discussion

First, one of the goals of our study was to provide independent constraints on the rheology of the asthenosphere and the interpretation of early postseismic displacements. We showed that values of the asthenopheric transient viscosity lower than $5\times10^{17}$ Pa.s, as previously proposed to explain deformation in the early postseismic stages (Gunawan et al., 2014; Kogan et al., 2013; Mikhailov et al., 2013; Pollitz, 2003; Pollitz et al., 2006; Sun et al., 2014), are in contradiction with the conclusions of our global seasonal deformation model. The observed fast early postseismic motions either might be due to afterslip and/or may indicate that the asthenospheric viscosity in active tectonics zone is lower than the Earth's average. However, note that there is no obvious correlation between zones of active tectonics and low admittance values (Figure S6), which seems to favor the first explanation. Indeed, because rapid relaxation and afterslip induce signals decaying rather differently with distance to the epicenter, Klein et al. (2016) inverted simultaneously for afterslip on the ruptured fault, creep in a low viscosity channel deeper along the plate interface, and relaxation in the asthenosphere after the Mw 8.8 Maule earthquake. Results from their study show that asthenospheric Burgers rheology parameters required to explain the early Maule postseismic motion include a $7 \times 10^{17}$ Pa.s transient viscosity, with a shear modulus equal to 4 times the elastic one, compatible with a range of seasonal deformation models, including an asthenopheric transient viscosity greater than $5 \times 10^{17}$ Pa.s (Figure 3c, dotted lines).

Then, the elastic structure of the Earth at time scales up to a few years has also been questioned independently by tidal studies using GNSS observations. Bos et al. (2015) proposed a reduction of the shear modulus of ~10% in the asthenosphere for western Europe at the M2 tidal frequency, also suggested by Goes et al. (2000) at seismic frequencies. These results are in agreement with ours, regardless of the global Earth average asthenospheric viscosity derived from our study. Indeed, only relatively large anelastic deformation in the asthenosphere (larger or equal to the elastic one) can be detected using the wavelengths loads resolved by the GRACE mission. With a quality factor Q independent of frequency, as proposed by Bos et al. (2015), the shear modulus reduction infered from the M2 oceanic tides but interpolated at annual frequencies would be of 13% and thus undetectable in the GNSS signal induced by loads provided by the GRACE mission (see Figure S4). Inversely, a $10^{17}$ Pa.s viscosity in the asthenosphere would yield at M2 periods to an anelastic deformation inferior to 1% that could not be detected. Different physical mechanisms may hold for short time scale, low-amplitude viscoelasticity and attenuation (grain boundary sliding and dislocation drag),

and longer time scale, larger-amplitude transient deformation (viscous creep of a mixture of materials with different viscosities). The studies involving smaller-amplitude anelastic deformation neither contradict nor support our conclusions: they contribute to the description of mantle anelasticity for time scales and amplitudes of the plastic deformation different from those concerned by our study.

Finally, values derived for annual periods of loading in our study must be in agreement with studies at longer time scales. For example, Nield et al. (2014) derived from GNSS observations of the Earth's response to recent ice mass unloading in Antarctica an upper mantle viscosity ranging from $6 \times 10^{17}$ to $2 \times 10^{18}$ Pa.s which is at the lower end of the asthenospheric viscosities deduced from pluriannual postseismic motions but is in agreement with our constraint of a viscosity larger than $5 \times 10^{17}$ Pa.s. Annual hydrological loading provides constraints on relatively low transient viscosities. However, our results are transposable to multiples of the loading period simply by multiplying viscosities by the corresponding factor (e.g., the curves of Figure 3c hold for a 10 year loading period with viscosities $\eta_T = 10^{18}$ Pas and $\eta = 10^{18}$ Pa.s. The phase shift on the right part of 3c would then simply be multiplied by 10). As the time series of satellite gravity measurements become longer, records of multiannual hydrological signals, such as recent ice unloading or multiannual continental hydrological signals, become available. This type of mass variations may interestingly lead to constraints on asthenospheric viscosities of a few $10^{18}$ Pa.s such as required to explain postseismic observations during the years following large earthquakes.

## 7. Conclusions

In the present paper, we have tested whether the seasonal deformation of the Earth under atmospheric, oceanic and hydrological loading was compatible with the rather low transient viscosities proposed in number of postseismic studies, affecting comparabale spatiotemporal scales. The horizontal displacement components are found to be the most affected by the rheology of the asthenosphere. Our results show that transient viscosities in the asthenosphere lower than $5 \times 10^{17}$ Pa.s with a transient shear modulus smaller than the elastic one, and for an asthenospheric thickness greater that 100 km are not compatible with the seasonal displacements observed globally. These values provide an upper bound on the contribution of postseismic viscoelastic relaxation of the Earth using a Burgers rheology. Our results are compatible with the attenuation studies of the asthenosphere at seismological or tidal frequencies, involving plastic deformation of smaller amplitude, as well as with recent ice melting studies at longer loading periods.

**Acknowledgments**
This work benefits from gravity data processed by the CNES/GRGS (http://grgs.obsmip.fr/) and of GNSS data processed by the Nevada Geodetic Laboratory (http://geodesy.unr.edu/). This work was partially supported by NSF grant EAR-1345136, the Laboratorie de Recherche Commun "Yves Rocard" (ENS-CEA-CNRS), and CNRS/TOSCA grant 2925. We thank Matt King and one anonymous reviewer for providing useful comments and help improving this manuscript.

## References

Anderson, D., Ben-Menahem, A., & Archambeau, C. (1965). Attenuation of seismic energy in the upper mantle. *Journal of Geophysical Research*, *70*(6), 1441–1448.

Barbot, S., Fialko, Y., & Bock, Y. (2009). Postseismic deformation due to the Mw 6.0 2004 Parkfield earthquake: Stress-driven creep on a fault with spatially variable rate-and-state friction parameters. *Journal of Geophysical Research*, *114*, B07405. https://doi.org/10.1029/2008JB005748

Bassin, C. (2000). The current limits of resolution for surface wave tomography in North America. *Eos, Transactions American Geophysical Union*, *81*, F897.

Bettinelli, P., Avouac, J., Flouzat, M., Bollinger, L., Ramillien, G., Rajaure, S., & Sapkota, S. (2008). Seasonal variations of seismicity and geodetic strain in the Himalaya induced by surface hydrology. *Earth and Planetary Science Letters*, *266*, 332–344.

Bills, B. G., Adams, K. D., & Wesnousky, S. G. (2007). Viscosity structure of the crust and upper mantle in Western Nevada from isostatic rebound patterns of the late Pleistocene Lake Lahontan high shoreline. *Journal of Geophysical Research*, *112*, B06405. https://doi.org/10.1029/2005JB003941

Bills, B. G., & May, G. M. (1987). Lake Bonneville: Constraints on lithospheric thickness and upper mantle viscosity from isostatic warping of Bonneville, Provo, and Gilbert stage shorelines. *Journal of Geophysical Research*, *92*, 11,493–11,508. https://doi.org/10.1029/JB092iB11p11493

Blewitt, G., Lavallee, D., Clarke, P., & Nurutdinov, K. (2001). A new global mode of Earth deformation: Seasonal cycle detected. *Science*, *294*, 2342–2345.

Bos, M. S., Penna, N. T., Baker, T. F., & Clarke, P. J. (2015). Ocean tide loading displacements in western Europe: 2. GPS-observed anelastic dispersion in the asthenosphere. *Journal of Geophysical Research: Solid Earth*, *120*, 6540–6557. https://doi.org/10.1002/2015JB011884

Burgmann, R., & Dresen, G. (2008). Rheology of the lower crust and upper mantle: Evidence from rock mechanics, geodesy, and field observations. *Annual Review of Earth and Planetary Sciences*, *36*, 531–567.

Caron, L., Métivier, L., Greff-Lefftz, M., Fleitout, L., & Rouby, H. (2017). Inverting glacial isostatic adjustment signal using Bayesian framework and two linearly relaxing rheologies. *Geophysical Journal International*, *209*(2), 1126–1147.

Carrère, L., & Lyard, F. (2003). Modeling the barotropic response of the global ocean to atmospheric wind and pressure forcing-comparisons with observations. *Geophysical Research Letters*, *30*(6), 1275. https://doi.org/10.1029/2002GL016473

Chanard, K. (2015). Seasonal deformation of the Earth, impact on seismicity (PhD Ecole Normale Superieure). Paris, France.

Chanard, K., Avouac, J., Ramillien, G., & Genrich, J. (2014). Modeling deformation induced by seasonal variations of continental water in the Himalaya region: Sensitivity to Earth elastic structure. *Journal of Geophysical Research: Solid Earth*, *119*, 5097–5113. https://doi.org/10.1002/2013JB010451

Chandrasekhar, D., Bürgmann, R., Reddy, C., Sunil, P., & Schmidt, D. A. (2009). Weak mantle in NW India probed by geodetic measurements following the 2001 Bhuj earthquake. *Earth and Planetary Science Letters*, *280*(1), 229–235.
Chen, J., Wilson, C., Tapley, B., & Grand, S. (2007). GRACE detects coseismic and postseismic deformation from the Sumatra-Andaman earthquake. *Geophysical Research Letters*, *34*, L13302. https://doi.org/10.1029/2007GL030356
Chopra, P. (1997). High-temperature transient creep in olivine rocks. *Tectonophysics*, *279*(104), 93–111.
Craig, T., Calais, E., Fleitout, L., Bollinger, L., & Scotti, O. (2016). Evidence for the release of long-term tectonic strain stored in continental interiors through intraplate earthquakes. *Geophysical Research Letters*, *43*, 6826–6836. https://doi.org/10.1002/2016GL069359
Davis, J., Elósegui, P., Mitrovica, J., & Tamisiea, M. (2004). Climate-driven deformation of the solid Earth from GRACE and GPS. *Geophysical Research Letters*, *31*, L24605. https://doi.org/10.1029/2004GL021435
DeVries, P. M., & Meade, B. J. (2013). Earthquake cycle deformation in the Tibetan plateau with a weak mid-crustal layer. *Journal of Geophysical Research: Solid Earth*, *118*, 3101–3111. https://doi.org/10.1002/jgrb.50209
Doin, M.-P., Twardzik, C., Ducret, G., Lasserre, C., Guillaso, S., & Jianbao, S. (2015). InSAR measurement of the deformation around Siling Co Lake: Inferences on the lower crust viscosity in central Tibet. *Journal of Geophysical Research: Solid Earth*, *120*, 5290–5310. https://doi.org/10.1002/2014JB011768
Dumoulin, C., Doin, M.-P., & Fleitout, L. (1999). Heat transport in stagnant lid convection with temperature-and pressure-dependent Newtonian or non-Newtonian rheology. *Journal of Geophysical Research*, *104*(B6), 12,759–12,777.
Dziewonski, A., & Anderson, D. (1981). Preliminary reference Earth model. *Physics of the Earth and Planetary Interiors*, *25*, 297–356.
Fialko, Y. (2004). Evidence of fluid-filled upper crust from observations of postseismic deformation due to the 1992 Mw7. 3 Landers earthquake. *Journal of Geophysical Research*, *109*, B08401. https://doi.org/10.1029/2004JB002985
Freed, A. M. (2007). Afterslip (and only afterslip) following the 2004 Parkfield, California, earthquake. *Geophysical Research Letters*, *34*, L06312. https://doi.org/10.1029/2006GL029155
Freed, A. M., & Bürgmann, R. (2004). Evidence of power-law flow in the Mojave desert mantle. *Nature*, *430*(6999), 548–551.
Fu, Y., Argus, D. F., Freymueller, J. T., & Heflin, M. B. (2013). Horizontal motion in elastic response to seasonal loading of rain water in the Amazon basin and monsoon water in Southeast Asia observed by GPS and inferred from GRACE. *Geophysical Research Letters*, *40*, 6048–6053. https://doi.org/10.1002/2013GL058093
Fu, Y., & Freymueller, J. T. (2012). Seasonal and long-term vertical deformation in the Nepal Himalaya constrained by GPS and GRACE measurements. *Journal of Geophysical Research*, *117*, B03407. https://doi.org/10.1029/2011JB008925
Fu, Y., Freymueller, J. T., & Jensen, T. (2012). Seasonal hydrological loading in southern Alaska observed by GPS and GRACE. *Geophysical Research Letters*, *39*, L15310. https://doi.org/10.1029/2012GL052453
Goes, S., Govers, R., & Vacher, P. (2000). Shallow mantle temperatures under Europe from *P* and *S* wave tomography. *Journal of Geophysical Research*, *105*(B5), 11153–11169.
Gunawan, E., Sagiya, T., Ito, T., Kimata, F., Tabei, T., Ohta, Y., et al. (2014). A comprehensive model of postseismic deformation of the 2004 Sumatra–Andaman earthquake deduced from GPS observations in Northern Sumatra. *Journal of Asian Earth Sciences*, *88*, 218–229.
Han, S.-C., Shum, C., Bevis, M., Ji, C., & Kuo, C.-Y. (2006). Crustal dilatation observed by GRACE after the 2004 Sumatra-Andaman earthquake. *Science*, *313*(5787), 658–662.
Han, S.-C., Sauber, J., Luthcke, S. B., Ji, C., & Pollitz, F. F. (2008). Implications of postseismic gravity change following the great 2004 Sumatra-Andaman earthquake from the regional harmonic analysis of GRACE intersatellite tracking data. *Journal of Geophysical Research*, *113*, B11413. https://doi.org/10.1029/2008JB005705
Hanson, D. R., & Spetzler, H. A. (1994). Transient creep in natural and synthetic, iron-bearing olivine single crystals: Mechanical results and dislocation microstructures. *Tectonophysics*, *235*(4), 293–315.
Ingleby, T., & Wright, T. (2017). Omori-like decay of postseismic velocities following continental earthquakes. *Geophysical Research Letters*, *44*, 3119–3130. https://doi.org/10.1002/2017GL072865
Ivins, E. R. (1996). Transient creep of a composite lower crust: 2. A polymineralic basis for rapidly evolving postseismic deformation modes. *Journal of Geophysical Research*, *101*(B12), 28,005–28,028.
Klein, E., Fleitout, L., Vigny, C., & Garaud, J. (2016). Afterslip and viscoelastic relaxation model inferred from the large-scale post-seismic deformation following the 2010 Mw 8.8 Maule earthquake (Chile). *Geophysical Journal International*, *205*(3), 1455–1472.
Kogan, M. G., Vasilenko, N. F., Frolov, D. I., Freymueller, J. T., Steblov, G. M., Prytkov, A. S., & Ekström, G. (2013). Rapid postseismic relaxation after the great 2006–2007 Kuril earthquakes from GPS observations in 2007–2011. *Journal of Geophysical Research: Solid Earth*, *118*, 3691–3706. https://doi.org/10.1002/jgrb.50245
Lambeck, K., Smither, C., & Johnston, P. (1998). Sea-level change, glacial rebound and mantle viscosity form northern Europe. *Geophysical Journal International*, *134*(1), 102–144.
Larsen, C. F., Motyka, R. J., Freymueller, J. T., Echelmeyer, K. A., & Ivins, E. R. (2005). Rapid viscoelastic uplift in southeast Alaska caused by post-little ice age glacial retreat. *Earth and Planetary Science Letters*, *237*(3), 548–560.
Lemoine, J.-M., Bruinsma, S., Loyer, S., Biancale, R., Marty, J.-C., Perosanz, F., & Balmino, G. (2007). Temporal gravity field models inferred from GRACE data. *Advances in Space Research*, *39*(10), 1620–1629.
Marone, C., Scholz, C., & Bilham, R. (1991). On the mechanics of earthquake afterslip. *Journal of Geophysical Research*, *96*(B5), 8441–8452.
Mikhailov, V., Lyakhovsky, V., Panet, I., van Dinther, Y., Diament, M., Gerya, T., et al. (2013). Numerical modelling of post-seismic rupture propagation after the Sumatra 26.12. 2004 earthquake constrained by GRACE gravity data. *Geophysical Journal International*, *194*(2), 640–650.
Nahmani, S., Bock, O., Bouin, M.-N., Santamaría-Gómez, A., Boy, J.-P., Collilieux, X., et al. (2012). Hydrological deformation induced by the West African monsoon: Comparison of GPS, GRACE and loading models. *Journal of Geophysical Research*, *117*, B05409. https://doi.org/10.1029/2011JB009102
Nield, G. A., Barletta, V. R., Bordoni, A., King, M. A., Whitehouse, P. L., Clarke, P. J., et al. (2014). Rapid bedrock uplift in the Antarctic Peninsula explained by viscoelastic response to recent ice unloading. *Earth and Planetary Science Letters*, *397*, 32–41.
Ogawa, R., & Heki, K. (2007). Slow postseismic recovery of geoid depression formed by the 2004 Sumatra-Andaman earthquake by mantle water diffusion. *Geophysical Research Letters*, *34*, L06313. https://doi.org/10.1029/2007GL029340
Perfettini, H., & Avouac, J.-P. (2004). Postseismic relaxation driven by brittle creep: A possible mechanism to reconcile geodetic measurements and the decay rate of aftershocks, application to the Chi-Chi earthquake, Taiwan. *Journal of Geophysical Research*, *109*, B02304. https://doi.org/10.1029/2003JB002488
Pollitz, F. F. (2003). Transient rheology of the uppermost mantle beneath the Mojave desert, California. *Earth and Planetary Science Letters*, *215*(1), 89–104.
Pollitz, F. F., Bürgmann, R., & Banerjee, P. (2006). Post-seismic relaxation following the great 2004 Sumatra-Andaman earthquake on a compressible self-gravitating earth. *Geophysical Journal International*, *167*(1), 397–420.

Pollitz, F. F., & Thatcher, W. (2010). On the resolution of shallow mantle viscosity structure using postearthquake relaxation data: Application to the 1999 Hector Mine, California, earthquake. *Journal of Geophysical Research*, *115*, B10412. https://doi.org/10.1029/2010JB007405

Post, R. (1977). High-temperature creep of Mt. Burnet Dunite. *Tectonophysics*, *42*, 75–110.

Raj, R. (1975). Transient behavior of diffusion-induced creep and creep rupture. *Metallurgical Transactions A*, *6*(8), 1499–1509.

Ramillien, G., Frappart, F., Cazenave, A., & Güntner, A. (2005). Time variations of land water storage from an inversion of 2 years of GRACE geoids. *Earth and Planetary Science Letters*, *235*, 283–301.

Ryder, I., Bürgmann, R., & Pollitz, F. (2011). Lower crustal relaxation beneath the Tibetan Plateau and Qaidam Basin following the 2001 Kokoxili earthquake. *Geophysical Journal International*, *187*(2), 613–630.

Savage, J., Lisowski, M., & Svarc, J. (1994). Postseismic deformation following the 1989 (Mw 7.1) Loma Prieta, California, earthquake. *Journal of Geophysical Research*, *99*(B7), 13,757–13,765.

Sigmundsson, F. (1991). Post-glacial rebound and asthenosphere viscosity in Iceland. *Geophysical Research Letters*, *18*(6), 1131–1134.

Smith, M. L, & Dahlen, F. A. (1981). The period and Q of the Chandler wobble. *Geophysical Journal International*, *64*(1), 223–281.

Steigenberger, P., Boehm, J., & Tesmer, V. (2009). Comparison of GMF/GPT with VMF1/ECMWF and implications for atmospheric loading. *Journal of Geodesy*, *83*(10), 943–951.

Sun, T., Wang, K., Iinuma, T., Hino, R., He, J., Fujimoto, H., et al. (2014). Prevalence of viscoelastic relaxation after the 2011 Tohoku-Oki earthquake. *Nature*, *514*(7520), 84–87.

Tapley, B., Ries, J., Bettadpur, S., Chambers, D., Cheng, M., Condi, F., et al. (2005). GGM02—An improved Earth gravity field model from GRACE. *Journal of Geodesy*, *79*(8), 467–478.

Thatcher, W., & Pollitz, F. F. (2008). Temporal evolution of continental lithospheric strength in actively deforming regions. *GSA Today*, *18*(4/5), 4–11.

Trubienko, O., Garaud, J.-D., & Fleitout, L. (2014). Models of postseismic deformation after megaearthquakes: The role of various rheological and geometrical parameters of the subduction zone. *Solid Earth Discussions*, *6*(1), 427–466.

Van Dam, T., Wahr, J., Milly, P., Shmakin, A., Blewitt, G., Lavallee, D., & Larson, K. (2001). Crustal displacements due to continental water loading. *Geophysical Research Letters*, *28*, 651–654.